Received: 16 March 2021 | Revised: 12 August 2021 | Accepted: 21 September 2021

DOI: 10.1002/suco.202100162

ARTICLE

fib CEB-FIP WILEY

A unified approach for determining the strength of FRC beams subjected to torsion–Part II: Analytical modeling

Luca Facconi[1] | **Ali Amin**[2] | **Fausto Minelli**[1] | **Giovanni Plizzari**[1]

[1]Department of Civil, Environmental, Architectural Engineering and Mathematics (DICATAM), University of Brescia, Brescia, Italy

[2]School of Civil Engineering, The University of Sydney, Sydney, New South Wales, Australia

Correspondence
Fausto Minelli, Department of Civil, Environmental, Architectural Engineering and Mathematics (DICATAM), University of Brescia, Brescia, Italy.
Email: fausto.minelli@unibs.it

Abstract

The addition of fibers to structural concrete is an accepted means in academia and practice to traverse tension across cracks. Several international codes of practice contain provisions, which allow a designer to rely on the fibers to resist flexure and shear. However, despite the wider community appreciating that the presence of fibers can significantly increase the capacity of reinforced concrete in resisting torsion, design guidelines are currently unavailable to the practicing engineer. As a result of minimum reinforcement requirements prescribed by codes to prevent excessive torsional cracking in reinforced concrete, a significant underutilization of the fibers is often encountered and this can lead to costly and exorbitant designs. In the accompanying paper, benchmark experimental data were presented on 18 large-scale fiber-reinforced concrete (FRC) members subjected to torsion, which clearly identified the beneficial effects of the fibers at all stages of loading. In this study, simplified and advanced mechanically consistent analytical models are developed within the so-called level of approximation approach (within the framework of current Model Code) to describe the strength of FRC beams loaded in torsion.

KEYWORDS

analytical model, fiber-reinforced concrete, finite element modeling, level of approximation, model code, torque–moment interaction, torsion, torsional resistance

1 | INTRODUCTION

Torsional moments develop in a multitude of concrete structures. These may be induced through the spatial geometry of the structure or through eccentrically applied loads. Torsion rarely acts alone and is usually combined with concurrent bending moments and/or transverse shears, and sometimes with axial forces too. The behavior of reinforced concrete (RC) elements subjected to torsion is not linear. Furthermore, if an under RC element cracks in torsion, the element's stiffness will dramatically reduce—much more so than if the element cracked in flexure.

The nonlinear stress distribution of the shear stresses distributed over the cross section of a concrete member subjected to torsion lends itself to the use of the so-called space truss analogy. Equations for the space truss analogy

Discussion on this paper must be submitted within two months of the print publication. The discussion will then be published in print, along with the authors' closure, if any, approximately nine months after the print publication.

in RC were first developed by Rausch.[1] In this approach, shear stresses are treated as constant over a finite thickness t_c, around the perimeter of the member. This allows for the beam to be represented as an equivalent hollow tube. As in the case of members loaded in shear, it was assumed that after cracking, the concrete can carry no tension and that an internal truss is developed within the beam. The truss contains longitudinal chords, and walls composed of concrete struts and transverse stirrup reinforcement.

For steel fiber-reinforced concrete (SFRC), however, it is well established that the fibers may provide concrete with a reliable means of traversing tension across cracks. This has been successfully demonstrated in experimental and analytical investigations not only at the material constitutive level but also in large-scale elements.[2–5] Confidence of the material in academia and in industry has resulted in the development of mechanically consistent expressions, which are available to the practicing engineer in international codes of practice for shear and flexure.[6,7] However, despite the wider community appreciating that the presence of fibers can significantly enhance the torsional behavior of RC elements, design guidelines are currently unavailable to the practicing engineer. Currently, some codes of practice suggest that torsion can be dealt with at the ultimate limit state by providing a minimum amount of reinforcement in the form of stirrups and longitudinal bars (i.e., within the space truss) to prevent excessive cracking.[6] Although this method can lead to safe solutions, this prescriptive approach can lead to unnecessarily large amounts of costly, manually placed, transverse reinforcement to be included within concrete structures. For SFRC members, this results in a significant underutilization of the fibers.

To that end, this article presents within the framework of the level of approximation (LoA) approach (see Muttoni and Ruiz[8]) towards a mechanically consistent means of quantifying and describing the strength of FRC members subjected to torsion.

2 | ANALYTICAL MODELING

Amin and Bentz[9] developed a simple yet rational approach to predict the strength of SFRC members subjected to pure torsion. Their model is an adaptation of the space truss approach for RC beams as introduced above, in which the capacity of fibers to transmit tension across cracks was incorporated. This is contrary to the traditional space truss approach for RC beams where the contribution of the concrete in tension is discounted after cracking. Not explicitly accounted for in the approach by Amin and Bentz[9] was the determination of the torsional resistance of members not containing links/stirrups, which may be economically attractive, as the placement of these reinforcements can be laborious. In this article, the model of Amin and Bentz[9] is used as a basis to determine the strength of SFRC beams subjected to either torsion or torsion in combination with other actions. The model has been calibrated to provide reasonable predictions even in the case of members that do not contain links/stirrups.

In the discussion below, one may note that pure torsion in concrete structures rarely occurs without other actions, and typically, flexure, shear, and/or axial forces may also be present within the structural system. By way of example, consider the illustration of a segment of a cracked SFRC beam with an overall height h and width b subjected to a torque T as shown in Figure 1a. Spiral cracks develop at an angle θ_v around the perimeter of the member. These cracks form in the same direction as a field of compressive stresses, or concrete struts, which resist the applied torque. The compressive stresses have a tangential and a normal component. The normal component of these compressive stresses induces a force into the longitudinal reinforcement (see Figure 1b). The tangential component of the compression field induces an average shear flow q within the member that equilibrates the applied torque. Equilibrium of the shearing stresses along the sections equivalent hollow tube (see Figure 1c) requires

$$T = 2qA_o, \tag{1}$$

where $A_o$is the area enclosed by the centerline of the shear flow path and is taken as $A_o = (b - t_c)(h - t_c)$ refer to Figure 1c. Testing by Amin and Bentz[9] and Facconi et al.[10,11] highlighted the benefits of fibers in preventing cover spalling in FRC members subjected to torsion. Therefore, unlike space truss models for plain RC, which wholly or partially discount the concrete cover in resisting the applied torsion, T,[12] in this article, we assume the thickness of the equivalent hollow tube section, t_c in FRC members as

$$t_c = 0.75\frac{A_g}{p}, \tag{2}$$

where $A_g = bh$ is the gross area of the concrete section and $p = 2(b + h)$ is the perimeter of the gross concrete cross section.[13]

In the determination of the ultimate shear flow, and hence the ultimate torsional capacity, Amin and Bentz[9] postulated that the failure of a member subjected to torsion is governed by the "weakest" component of the space truss. That is, failure is governed either by yielding

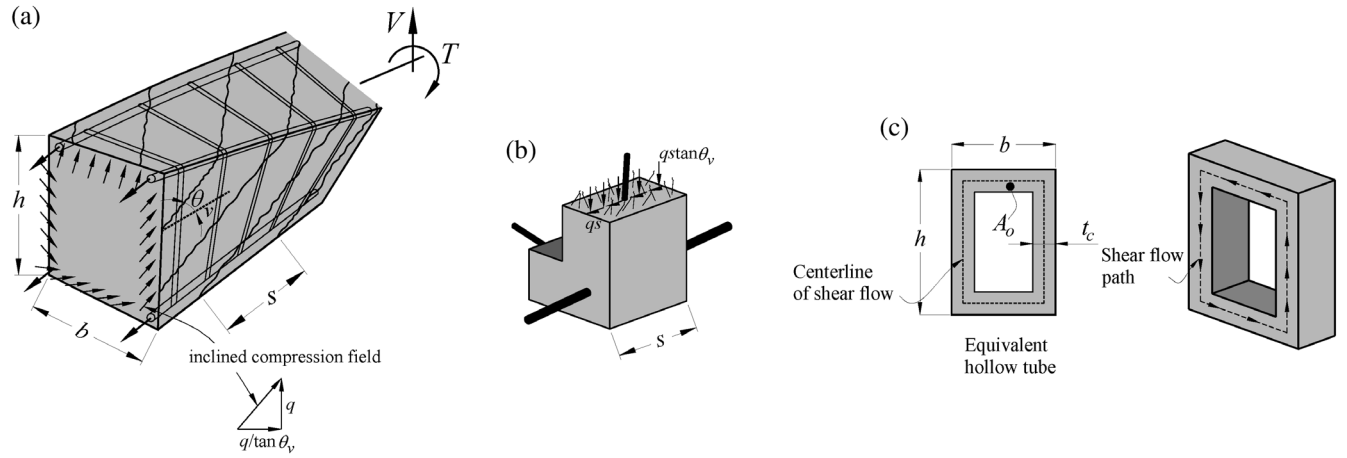

FIGURE 1 Cracked steel fiber-reinforced concrete (SFRC) beam in torsion

of the longitudinal steel or by yielding of the transverse web steel (if present) or from crushing of the compressive concrete strut. From the equilibrium of a typical element of the space truss (see Figure 1), incorporating the effect of the fibers bridging the crack, Amin and Bentz[9] expressed Equation (1) as

$$T = 2A_o \times \min\left(\begin{array}{c}\left(\frac{A_{sv}f_{sy,v}}{s}+t_c f_w\right)\cot\theta_v \\ \left(\frac{\sum A_{sl,i}f_{sy,l,i}}{p}+t_c f_w\right)\tan\theta_v\end{array}\right) \le 0.25 f_{cm}\frac{1.7A_g^2}{p}, \quad (3)$$

where f_{cm} is the mean cylindrical concrete compressive strength, $f_{sy,v}$ and s are the yield strength and spacing of the transverse steel reinforcement, respectively, A_{sv} is taken as the area of one leg of the transverse reinforcement, and A_{sl} and $f_{sy,l}$ denote the cross-sectional area and yield strength of each longitudinal steel bar, respectively. The limiting term of Equation (3) is included to ensure the yielding of the steel reinforcement occurs prior to crushing of the concrete.[13] It is important to note from a detailing perspective that, for the space truss to be fully effective, the longitudinal steel (at the top and bottom of the section) must be well anchored at each corner of the cross section beyond the length of the section that is subjected to torsion.

The contribution of the steel fibers to the strength of FRC beams loaded in torsion is included in Equation (3) through the term f_w, which defines the residual tensile strength provided by the fibers over a plane of unit area. The residual strength offered by the fibers is predominately a function of the supplied fiber dosage, fiber type, and concrete matrix. The tension that may be transmitted by the fibers is dependent on the mean width of the crack under consideration, w. From a material constitutive point, the post-cracking tensile stress that the fibers can transmit can be directly obtained from uniaxial tension test data, from constitutive models reported by codes (e.g., *fib* Model Code 2010 and AS3600[6,7]) or gathered following an inverse analysis procedure of prism bending or round panel specimens (e.g., see[14–16]). In the analysis of structural members containing fibers, it is assumed that the tensile stress carried by the fibers acts uniformly along the thickness of the equivalent hollow tube section, t_c.

In the evaluation of Equation (3), it is clear that physically consistent expressions must be conceived for the stress carried by the fibers, f_w and the angle of the compressive strut, θ_v. Depending on the level of detail required at the time of calculation (i.e., during preliminary sizing design, detailed design or in the strength evaluation of members, etc.), along with the importance of the structural element, the more or less refined the physical model should be. In the preliminary sizing of members, quick, efficient, and consistent solutions are usually required. However, when evaluating the capacity of existing structures, more refined models may be required to gain a full understanding of the structure's behavior. This rationale has been introduced in recent codes of practice (e.g.,[6,7]) by means of a LoA) approach. The higher the LoA, the greater the design effort is required. That said, however, equations for a lower tier of the LoA approach should be able to be directly derived from higher levels without compromising the physical meaning behind the key variables. This is also the rationale adopted in the following where three accuracy levels are proposed.

The proposed LoA I approach provides a quick, "back of the envelope" method for the determination of the torsional strength of SFRC members. This approach is based

on simplifications made to the proposed LoA II approach. The LoA II approach provides more insight into the governing variables than the LoA I approach and is more suited to be solved using a simple spreadsheet. The LoA III approach is developed within the context of the finite element method.

In the following, the LoA II approximation is first developed within the framework of the model introduced above by Amin and Bentz.[9] The LoA I is then developed following simplifications made within this framework.

2.1 | Level II approximation

Early studies on torsion in plain RC assumed the compression field angle θ_v at failure to be 45°.[17] The Simplified Modified Compression Field Theory (MCFT)[18] for shear critical members, hereafter referred to as SMCFT, predicts θ_v as a function of the longitudinal strain at cross section mid-height ε_x:

$$\theta_{v,SMCFT} = 29^\circ + 7000\varepsilon_x \tag{4}$$

Facconi et al.[10,19] found that $\theta_{v,SMCFT}$ is underestimated for large-scale SFRC beams with little or no transverse reinforcement failing in pure torsion. Such an underestimation of θ_v may lead to unsafe solutions. In these instances, the critical crack would inherently be assumed to pass through multiple stirrups/links, which may not be the case in reality. To this end, based on the experimental results summarized and discussed in the accompanying paper,[19] a modified expression for θ_v has been calibrated for beams subjected to torsion:

$$\theta_{v,proposed} = 38.5^\circ + 4000\varepsilon_x. \tag{5}$$

Comparing Equations (4) and (5), it is noted that for loading and geometrical configurations where torsional moments govern, Equation (5) yields strut angles close to 45°, which is more representative than those obtained through Equation (4).

For non-prestressed members subjected to torsion, the Canadian Standards Association[20] equation for ε_x for combined shear and torsion is

$$\varepsilon_x = \frac{M/d + \sqrt{V^2 + \left(\frac{0.9Tp}{2A_o}\right)^2} + 0.5N}{2E_sA_s}, \tag{6}$$

where N is the axial load normal to the cross section, V and M are the shear force and the bending moment resisted by the beam, respectively, A_s is the total area of the longitudinal reinforcement contained within the flexural tension side, E_s is the Young's modulus of reinforcing steel, and d is the effective depth of the beam. For members subjected to pure torsion (i.e., where $N = M = V = 0$), Equation (6) reduces to

$$\varepsilon_x = \frac{0.9Tp}{2A_oE_s(A_{sB} + A_{sT})}, \tag{7}$$

where A_{sB} and A_{sT} are the total cross-sectional area of longitudinal steel at the bottom and top half of the beam cross section, respectively (assuming the member is unsymmetrically reinforced in the longitudinal direction).

The average width of the crack at the mid-height of the section, w, is related to the longitudinal strain parameter, ε_x. The SMCFT[18] predicts this relationship for shear critical specimens as

$$w_{SMFCT} = 0.2 + 1000\varepsilon_x \geq 0.125\,\text{mm}, \tag{8}$$

Similarly, Facconi et al.[10,19] found this expression to significantly overpredict the width of the localized crack at peak load. To fit in line with the results of the experiments of this research program, the following modified expression for w has been calibrated for specimens subjected to torsion:

$$w_{proposed} = 0.10 + 550\varepsilon_x \geq 0.50\,\text{mm}. \tag{9}$$

We note that for softening FRC, as is typically adopted in practice, the limiting term of Equation (9) provides a conservative, minimum crack width, for which the fibers are effective.

Consistent with the model by Amin and Bentz,[9] the strain and, hence, crack width at the mid-depth of the section are used to determine the average fiber stress contribution component over the length of the crack.

The discussion so far pertains to members including longitudinal and transverse steel reinforcement where the failure of the member corresponds to yielding of either type of reinforcement (provided crushing does not occur). For the case where stirrups are not included in the member, the failure of the member is governed predominantly by the pullout of the fibers across the dominant crack. Consider again the shear flow path as shown in Figure 1. Equilibrium in the longitudinal direction of the beam allows for the determination of the stress developed in the longitudinal reinforcement as a function of the applied torque:

$$f_{sl} = \frac{Tp\cot\theta_v}{2A_o(A_{sB} + A_{sT})} \leq f_{sy,L}. \tag{10}$$

Similarly, the stress in each leg of the stirrup reinforcement (if present) can be expressed as

$$f_{sv} = \frac{Ts \tan \theta_v}{2A_{sv}A_o} \leq f_{sy,v}. \quad (11)$$

Recent research[21,22] has highlighted the beneficial effect of including fibers in concrete in the transfer of shear stresses across cracks. It was analytically shown by Kaufmann et al.[21] that the fibers enhance the interlocking of aggregates along the crack face. To more accurately account for the transmission of stress across cracks through aggregate interlock in the LoA II approach, Equation (3) is rewritten as

$$T = 2A_o \times \min \left(\begin{array}{c} \left(\frac{A_{sw} f_{sv}}{s} + t_c f_w \right) \cot \theta_v + t_c v_{ci} \tan \theta_v \\ \left(\frac{\sum A_{sl,i} f_{sl,i}}{p} + t_c f_w \right) \tan \theta_v + t_c v_{ci} \cot \theta_v \end{array} \right) \leq 0.25 f_{cm} \frac{1.7 A_g^2}{p}, \quad (12)$$

where v_{ci} is the shear stress along the cracked face and taken directly from the MCFT[23]:

$$v_{ci} = \frac{0.18\sqrt{f_{cm}}}{0.31 + \frac{24w}{a_g + 16}}, \quad (13)$$

where a_g is the maximum aggregate size.

Several approaches are available to determine the residual tensile strength of FRC from standard notched prism tests. For prisms tested according to EN14651,[24] the *fib* Model Code 2010[6] proposes the following simplified linear constitutive stress versus crack opening displacement relationship:

$$f_{w,fib} = f_{Fts} + \frac{f_{Fts} - f_{Ftu}}{w_{SLS} - w_u} \cdot (w - 0.5\,\text{mm}) = \frac{4}{3} w \cdot (0.285 f_{R3} - 0.315 f_{R1}) + 0.58 f_{R1} - 0.19 f_{R3}, \quad (14)$$

where f_{R1} and f_{R3} correspond to the residual flexural strength at a CMOD equal to 0.5 and 2.5 mm, respectively; f_{Fts} is the residual strength significant for service loading conditions; f_{Ftu} is the residual strength significant for ultimate conditions; w is the crack width in [mm]; $\text{CMOD}_3 = 2.5$ mm; $w_u = \text{CMOD}_3/2 = 1.25$ mm; $w_{SLS} = 0.5$ mm. As recommended by the latest draft Annex to prEN 1992(2019),[25] f_{Fts} and f_{Ftu} have been here calculated as $f_{Fts} = 0.37 f_{R1}$ and $f_{Ftu} = f_{Fts} - w_u (f_{Fts} - 0.57 f_{R3} + 0.26 f_{R1})/\text{CMOD}_3$.

Alternatively, the simplified model of Amin et al.[16] has been adopted in the Australian Standard for Concrete Structures[7]:

$$f_{w,\text{AS}} = \frac{f_{R2}}{3} + (f_{R4} - f_{R2})(0.43w - 0.25) \geq 0, \quad (15)$$

where f_{R2} and f_{R4} are the residual flexural strength at a CMOD of 1.5 and 3.5 mm, respectively.

The LoA II solution for the maximum torque, T, that may be resisted by the member is obtained by initially guessing values for ε_x and T. The crack width, w, and angle of the compressive strut, θ_v, are then calculated through Equations (9) and (5), respectively. The crack width allows determining the tensile strength of the SFRC by a uniaxial constitutive law relating f_w to w through either Equation (14) or (15). Based on the guessed value of T, the stress in the longitudinal and stirrup reinforcements may be obtained through Equations (10) and (11), respectively. The contribution of aggregate interlock along the cracked face can be evaluated through Equation (13). Equation (12) can then be deployed to evaluate T, which, in turn, allows to calculate ε_x by using Equation (7). The process is iterated until convergence of ε_x and T. This process is summarized in the flowchart presented in Figure 2.

2.2 | Level I approximation

The main goal in the development of the LoA II approach derived above was that it could be reduced back to a simple equation using logical assumptions. To avoid the complexity associated with iterating through Equations (5) to (14) above and to make it more conducive for a "back of the envelope" calculation, two assumptions can be made to simplify Equation (12). The unknowns in this equation are the strut angle, θ_v, and the residual tensile strength offered by the fibers, f_w, and both are related to the longitudinal strain parameter, ε_x. Setting the strain at mid-depth on the member to 50% of the yield strain of the bottom layer of reinforcing steel gives $\varepsilon_x = 0.5 f_{sy,B}/E_s = 2.5 \times 10^{-6} f_{sy,B}$ (see *fib* Model Code 2010,[6] clause 7.3.3.2: Members without shear reinforcement—level I approximation). Such an assumption provides for some conservatism in the method. Substituting this value into Equations (5) and (9) gives $\theta_v = 38.5^\circ + 0.01 f_{sy,B}$ and $w = 0.1 + 0.001375 f_{sy,B}$, for class B and N steels typically used in Europe and Australia, respectively, $f_{sy} = 500$ MPa, and hence θ_v and w may be taken as 43.5° and 0.79 mm, respectively. Note that this simplification does not imply that the strength of a SFRC beam in pure torsion is directly proportional to the yield strength of the tensile steel, but rather, increasing the yield strength of the

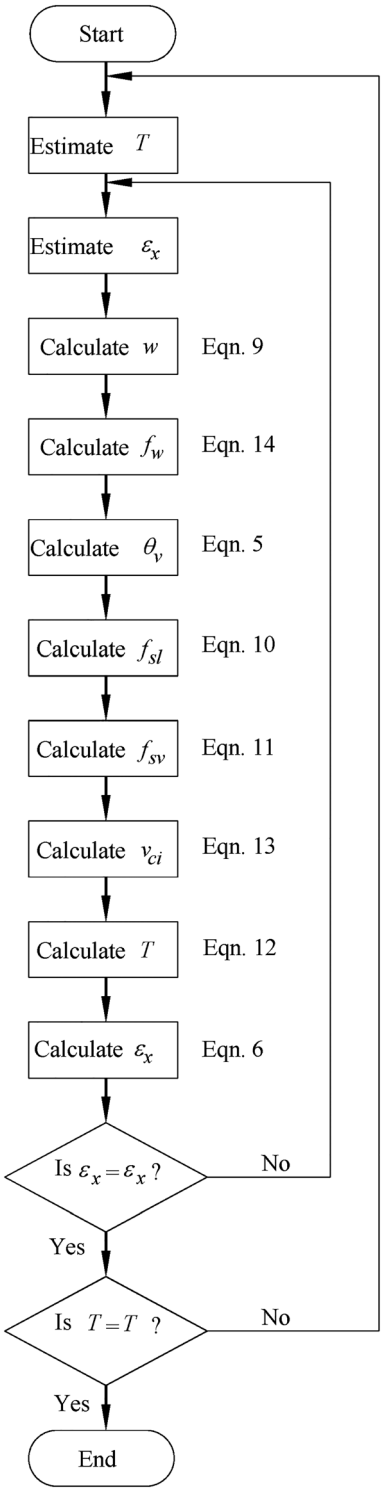

FIGURE 2 Procedure to solve the level of approximation (LoA) II method

longitudinal steel will lead to wider crack widths at the location of the steel, and at the mid-depth of the section. As a result, the contribution of the fibers decreases, as is the case for softening FRC.

The residual tensile stress carried by the fibers can be evaluated by substituting $w = 0.79$ into Equation 14. This gives $f_{w,\text{fib}} = 0.25f_{R1} + 0.11f_{R3}$ and $f_{w,\text{AS}} = 0.24f_{R2} + 0.09f_{R4}$. Examining the material data in the accompanying paper[19] and in Amin and Bentz,[9] the expressions above can be simplified to $f_w = 0.33f_{R3}$ without introducing significant error. Note that f_{R3} is the flexural strength of SFRC determined for a CMOD equal to 2.5 mm determined from notched prisms according to EN14651.[24]

To that end, for the LoA I approach, we adapt Equation (12) as

$$T = 2A_o \times \min \left(\begin{array}{l} \left(\frac{A_{sv} f_{sy,v}}{s} + 0.33\alpha t_c f_{R3} \right) \cot 43.5^{\circ} \\ \left(\frac{\sum A_{sl,i} f_{sy,l,i}}{p} + 0.33\alpha t_c f_{R3} \right) \tan 43.5^{\circ} \end{array} \right) \leq 0.25 f_{cm} \frac{1.7A_g^2}{p}, \tag{16}$$

The factor α is included in Equation (16) to account for the beneficial effects of the fibers in transmitting shear across cracks. For members containing transverse reinforcement, the transfer of shear across the crack is predominately transmitted through the reinforcement. However, for members without transverse reinforcement, this stress is carried by the fibers and through aggregate interlock. In this study, we take $\alpha = 1$ for FRC members with stirrups and $\alpha = 1.5$ for FRC members without stirrups and recognize that for FRC members containing stirrups, crack widths are likely to be wide enough that the beneficial influence of aggregate interlock is abated.

2.3 | Level III approximation

In the event that more refined analyses are necessary (i.e., in the design of complex critical elements or in the assessment of existing critical structures), a nonlinear analysis based on numerical methods may also be performed. The use of these methods is usually only justified where significant economic savings can be provided. It should not be understated that the results stemming from numerical tools can be sensitive to be the inputted parameters (i.e., the material constitutive laws and other built-in features of the numerical tool). As such, it is recommended that only experienced users, who can adequately assess and interpret the results of the simulations, rely on their outputs for design. Moreover, the results using these methods should

be carefully checked against predictions using the LoA II model and critically interpreted. In this article, the commercially available package ATENA[26] is deployed to investigate the response of a number of the beams tested in the accompanying paper.[19]

3 | MODEL VALIDATION

3.1 | Analytical solutions

The proposed LoA I and II models developed here are first compared to the 14 SFRC specimens tested in the accompanying paper[19] as well as the two SFRC torsion specimens tested by Amin and Bentz.[9] These specimens have been chosen as both datasets are complimented with a complete suite of material property tests, which quantify the post-cracking residual tensile strength offered by the fibers. A summary of the experimental data is presented in Tables 1 and 2, which report, among other properties, the total length l of the test beams, the yield strength of top ($f_{sy,T}$) and bottom ($f_{sy,B}$) longitudinal reinforcement and the residual flexural strengths f_{R1}, f_{R2}, f_{R3}, and f_{R4} obtained from characterization tests of SFRC carried out according to EN14651.[24] The results of the LoA I model are presented in Table 3. The results of the LoA II model are presented in Tables 4 and 5. Despite the simplicity of the LoA I model, a good correlation with the experimental data is observed, with a model-to-experiment ratio (T_{mod}/T_{exp}) of 0.83 and a CoV of 0.17. Such results provide a reasonable degree of conservatism in the model—particularly for the effort required in computation.

With regard to the LoA II model, the residual tensile strength offered by the fibers, f_w must be determined. Table 4 presents the results of the LoA II model using Equation (14) and Table 5 presents the results of the LoA II using Equation (15). As shown in Tables 4 and 5, good correlations between the model and the experimental data are observed with the exception of specimens TB17 and TB18, regardless of the f_w-w relationship adopted. These specimens are characterized by a flexural reinforcing ratio of $\rho_s = A_{sB}/bd = 0.132\%$, which is less than the minimum prescribed by the *fib* MC2010 ($\rho_{s,min} = \sim 0.165\%$) for flexure. For these specimens, the LoA II model predicts the longitudinal reinforcement to yield, which coincides with a very large crack widths, and steep strut angles and consequently the model breaks down. If all the beams are taken into consideration, the mean ratio (T_{mod}/T_{exp}) between the predicted and the experimental maximum torque using Equation (14) is equal to 0.94 (CoV = 0.11). On the contrary, by removing the beams TB17 and TB18 from the dataset (which are unlikely to be representative of those constructed in practice), a model-to-experiment ratio of 0.96 and a CoV of 0.09 is achieved. Similarly using Equation (15), the mean

TABLE 1 Geometric properties of specimens tested by Facconi et al.[19] and Amin and Bentz[9]

		Geometric properties						
Researchers	**Beam ID**	***b* [mm]**	***h* [mm]**	***l* [mm]**	A_{sB} [mm^2]	A_{sT} [mm^2]	A_{sv} [mm^2]	***s* [mm]**
Facconi et al.[21]	TB3-G25-L18	300	300	2700	510	510	-	-
	TB4-G25-L18	300	300	2700	510	510	-	-
	TB5-G50-L18	300	300	2700	510	510	-	-
	TB6-G50-L18	300	300	2700	510	510	-	-
	TB7-D25-L18	300	300	2700	510	510	-	-
	TB8-D25-L18	300	300	2700	510	510	-	-
	TB9-D50-L18	300	300	2700	510	510	-	-
	TB10-D50-L18	300	300	2700	510	510	-	-
	TB11-D50-L18-ST6/150	300	300	2700	510	510	28.3	150
	TB12-D50-L18-ST6/150	300	300	2700	510	510	28.3	150
	TB15-D50-L18-ST6/200	300	300	2700	510	510	28.3	200
	TB16-D50-L18-ST6/200	300	300	2700	510	510	28.3	200
	TB17-D50-L8	300	300	2700	510	510	-	-
	TB18-D50-L8	300	300	2700	510	510	-	-
Amin and Bentz[9]	T-30-8	200	280	1600	600	160	50	200
	T-30-10	200	280	1600	600	160	80	200

TABLE 2 Materials properties of specimens tested by Facconi et al.[19] and Amin and Bentz[9]

		Material properties							
Researchers	**Beam ID**	$f_{sy,B}$ [MPa]	$f_{sy,T}$ [MPa]	$f_{sy,v}$ [MPa]	f_{cm} [MPa]	f_{R1} [MPa]	f_{R2} [MPa]	f_{R3} [MPa]	f_{R4} [MPa]
Facconi et al.[21]	TB3-G25-L18	516	516	-	43.6	4.1	4.5	4.2	3.8
	TB4-G25-L18	516	516	-	43.6	4.1	4.5	4.2	3.8
	TB5-G50-L18	516	516	-	43.4	7.2	7.2	6.6	5.7
	TB6-G50-L18	516	516	-	43.4	7.2	7.2	6.6	5.7
	TB7-D25-L18	507	507	-	42.8	3.4	5.2	5.0	4.8
	TB8-D25-L18	507	507	-	42.8	3.4	5.2	5.0	4.8
	TB9-D50-L18	507	507	-	42.6	6.0	7.8	6.7	6.1
	TB10-D50-L18	507	507	-	42.6	6.0	7.8	6.7	6.1
	TB11-D50-L18-ST6/150	507	507	510	42.6	6.0	7.8	6.7	6.1
	TB12-D50-L18-ST6/150	507	507	510	42.6	6.0	7.8	6.7	6.1
	TB15-D50-L18-ST6/200	507	507	510	42.6	6.0	7.8	6.7	6.1
	TB16-D50-L18-ST6/200	507	507	510	42.6	6.0	7.8	6.7	6.1
	TB17-D50-L8	567	567	-	42.6	6.0	7.8	6.7	6.1
	TB18-D50-L8	567	567	-	42.6	6.0	7.8	6.7	6.1
Amin and Bentz[9]	T-30-8	532	538	567	42.3	3.1	3.5	3.5	3.2
	T-30-10	532	538	513	42.3	3.1	3.5	3.5	3.2

TABLE 3 Level of approximation (LoA) I predictions and comparisons to Facconi et al.[19] and Amin and Bentz[9] specimens

		LoA I									
Researchers	**Beam ID**	A_g [mm^2]	p_h [mm]	t_c [mm]	A_o [mm^2]	θ_v [°]	α [−]	f_w [MPa]	T_{mod} [kNm]	T_{exp} [kNm]	T_{mod}/T_{exp} [−]
Facconi et al.[21]	TB3-G25-L18	90,000	1200	56.25	59,414	43.5	1.5	1.39	14.64	27.32	0.54
	TB4-G25-L18	90,000	1200	56.25	59,414	43.5	1.5	1.39	14.64	22.94	0.64
	TB5-G50-L18	90,000	1200	56.25	59,414	43.5	1.5	2.18	23.01	26.94	0.85
	TB6-G50-L18	90,000	1200	56.25	59,414	43.5	1.5	2.18	23.01	24.63	0.93
	TB7-D25-L18	90,000	1200	56.25	59,414	43.5	1.5	1.66	17.54	20.27	0.87
	TB8-D25-L18	90,000	1200	56.25	59,414	43.5	1.5	1.66	17.54	20.85	0.84
	TB9-D50-L18	90,000	1200	56.25	59,414	43.5	1.5	2.21	23.33	27.92	0.84
	TB10-D50-L18	90,000	1200	56.25	59,414	43.5	1.5	2.21	23.33	25.20	0.93
	TB11-D50-L18-ST6/150	90,000	1200	56.25	59,414	43.5	1.0	2.21	27.60	35.63	0.77
	TB12-D50-L18-ST6/150	90,000	1200	56.25	59,414	43.5	1.0	2.21	27.60	32.03	0.86
	TB15-D50-L18-ST6/200	90,000	1200	56.25	59,414	43.5	1.0	2.21	24.59	33.95	0.72
	TB16-D50-L18-ST6/200	90,000	1200	56.25	59,414	43.5	1.0	2.21	24.59	33.37	0.74
	TB17-D50-L8	90,000	1200	56.25	59,414	43.5	1.5	2.21	23.33	22.03	1.06
	TB18-D50-L8	90,000	1200	56.25	59,414	43.5	1.5	2.21	23.33	22.02	1.06
Amin and Bentz[9]	T-30-8	56,000	960	43.75	36,914	43.5	1.0	1.16	14.99	21.00	0.71
	T-30-10	56,000	960	43.75	36,914	43.5	1.0	1.16	19.93	22.65	0.88
										Mean	0.83
										CoV	0.17

TABLE 4 LoA II predictions using Equation (14) and comparisons to Facconi et al.[19] and Amin and Bentz[9] specimens

		LoA II											
Researchers	**Beam ID**	ε_x [mm/m]	w [mm]	θ_v [°]	$f_{w,fib}$ [MPa]	f_{sl} [MPa]	f_{sv} [MPa]	ν_{ci} [MPa]	T_S [kNm]	T_L [kNm]	$T_{mod,fib}$ [kNm]	T_{exp} [kNm]	$T_{mod,fib}/T_{exp}$ [−]
Facconi et al.[21]	TB3-G25-L18	0.936	0.615	42.2	1.50	187	-	1.64	21.02	38.37	21.02	27.32	0.769
	TB4-G25-L18	0.936	0.615	42.2	1.50	187	-	1.64	21.02	38.37	21.02	22.94	0.916
	TB5-G50-L18	1.204	0.762	43.3	2.53	241	-	1.44	27.03	49.11	27.03	26.94	1.003
	TB6-G50-L18	1.204	0.762	43.3	2.53	241	-	1.44	27.03	49.11	27.03	24.63	1.097
	TB7-D25-L18	0.881	0.585	42.0	1.30	176	-	1.69	19.77	36.35	19.94	20.27	0.984
	TB8-D25-L18	0.881	0.585	42.0	1.30	176	-	1.69	19.77	36.35	19.94	20.85	0.956
	TB9-D50-L18	1.125	0.719	43.0	2.23	225	-	1.50	25.27	45.80	25.27	27.92	0.905
	TB10-D50-L18	1.125	0.719	43.0	2.23	225	-	1.50	25.27	45.80	25.27	25.20	1.003
	TB11-D50-L18-ST6/150	1.554	0.954	44.7	2.23	311	510	1.25	34.87	54.26	34.87	35.63	0.979
	TB12-D50-L18-ST6/150	1.554	0.954	44.7	2.23	311	510	1.25	34.87	54.26	34.87	32.03	1.089
	TB15-D50-L18-ST6/200	1.450	0.897	44.3	2.23	290	510	1.30	32.54	52.03	32.54	33.95	0.958
	TB16-D50-L18-ST6/200	1.450	0.897	44.3	2.23	290	510	1.30	32.54	52.03	32.54	33.37	0.975
	TB17-D50-L8	3.873	2.23	54.0	2.27	567	-	0.66	17.04	39.47	17.04	22.03	0.773
	TB18-D50-L8	3.873	2.23	54.0	2.27	567	-	0.66	17.04	39.47	17.04	22.02	0.784
Amin and Bentz[9]	T-30-8	1.385	0.862	44.0	1.16	277	567	1.06	17.98	22.79	17.98	21.00	0.856
	T-30-10	1.678	1.023	45.2	1.16	336	513	0.93	21.79	26.52	21.58	22.65	0.962
												Mean	0.94
												CoV	0.11

TABLE 5 LoA II predictions using Equation (15) and comparisons to Facconi et al.[19] and Amin and Bentz[9] specimens

		LoA II											
Researchers	**Beam ID**	ε_x [mm/m]	w [mm]	θ_v [°]	$f_{w,AS}$ [MPa]	f_{sl} [MPa]	f_{sv} [MPa]	v_{ci} [MPa]	T_S [kNm]	T_L [kNm]	$T_{mod,AS}$ [kNm]	T_{exp} [kNm]	$T_{mod,AS}/T_{exp}$ [−]
Facconi et al.[21]	TB3-G25-L18	0.933	0.613	42.2	1.49	186	-	1.64	20.94	38.25	20.94	27.32	0.766
	TB4-G25-L18	0.933	0.613	42.2	1.49	186	-	1.64	20.94	38.25	20.94	22.94	0.913
	TB5-G50-L18	1.146	0.738	43.1	2.30	229	-	1.48	25.72	46.64	25.72	26.94	0.955
	TB6-G50-L18	1.146	0.738	43.1	2.30	229	-	1.48	25.72	46.64	25.72	24.63	1.044
	TB7-D25-L18	0.995	0.647	42.5	1.72	199	-	1.59	22.32	40.57	22.32	20.27	1.101
	TB8-D25-L18	0.995	0.647	42.5	1.72	199	-	1.59	22.32	40.57	22.32	20.85	1.071
	TB9-D50-L18	1.191	0.755	43.3	2.48	238	-	1.45	26.72	48.52	26.72	27.92	0.957
	TB10-D50-L18	1.191	0.755	43.3	2.48	238	-	1.45	26.72	48.52	26.72	25.20	1.060
	TB11-D50-L18-ST6/150	1.575	0.966	44.8	2.32	315	510	1.24	35.32	55.35	35.32	35.63	0.991
	TB12-D50-L18-ST6/150	1.575	0.966	44.8	2.32	315	510	1.24	35.32	55.35	35.32	32.03	1.103
	TB15-D50-L18-ST6/200	1.481	0.915	44.4	2.36	296	510	1.28	33.25	53.54	33.25	33.95	0.979
	TB16-D50-L18-ST6/200	1.481	0.915	44.4	2.36	296	510	1.28	33.25	53.54	33.25	33.37	0.996
	TB17-D50-L8	3.345	1.940	51.9	1.61	567	-	0.74	14.74	31.92	14.74	22.03	0.669
	TB18-D50-L8	3.345	1.940	51.9	1.61	567	-	0.74	14.74	31.92	14.74	22.02	0.669
Amin and Bentz[9]	T-30-8	1.381	0.860	44.0	1.14	276	567	1.06	17.94	22.70	17.94	21.00	0.854
	T-30-10	1.669	1.018	45.2	1.12	334	513	0.93	21.68	26.27	21.68	22.65	0.957
												Mean	0.94
												CoV	0.15

ratio (T_{mod}/T_{exp}) is 0.94 (CoV = 0.14), and excluding TB17 and TB18 from the dataset gives a mean ratio (T_{mod}/T_{exp}) equal to 0.98 (CoV = 0.10). It is seen that the proposed LoA II model is very versatile as consistent results have been obtained regardless of the adopted f_w-w relationships.

3.2 | Finite element simulation predictions (level III approximation)

In this section, the results of a nonlinear finite element model are first compared to some of the beams tested in the accompanying paper.[19] This method of analysis is referred to the LoA III method. The SFRC members considered in this section are simulated using the fracture-plastic model "CC3DNonLinCementitious2User" implemented in the commercially available finite element software package ATENA.[26] Details of the test specimens are provided in Figure 3a. Figure 3b illustrates the adopted 3D numerical model including both counteracting torques (T) applied to the specimen ends, as well as two-point loads ($P/2$) used to introduce a constant bending moment (M = 600 mm·$P/2$) within the monitored central region of the specimen. In this analysis, the two torques (T) are applied through prescribed displacements acting at both ends of the member (see Figures 3b,c). The mesh consists of 2176 20-node isoparametric brick elements integrated by Gauss integration. The fracture behavior of the SFRC is modeled by an orthotropic smeared crack formulation based on fixed cracks and on the Rankine tensile criterion including a multilinear stress–strain softening law. The plasticity

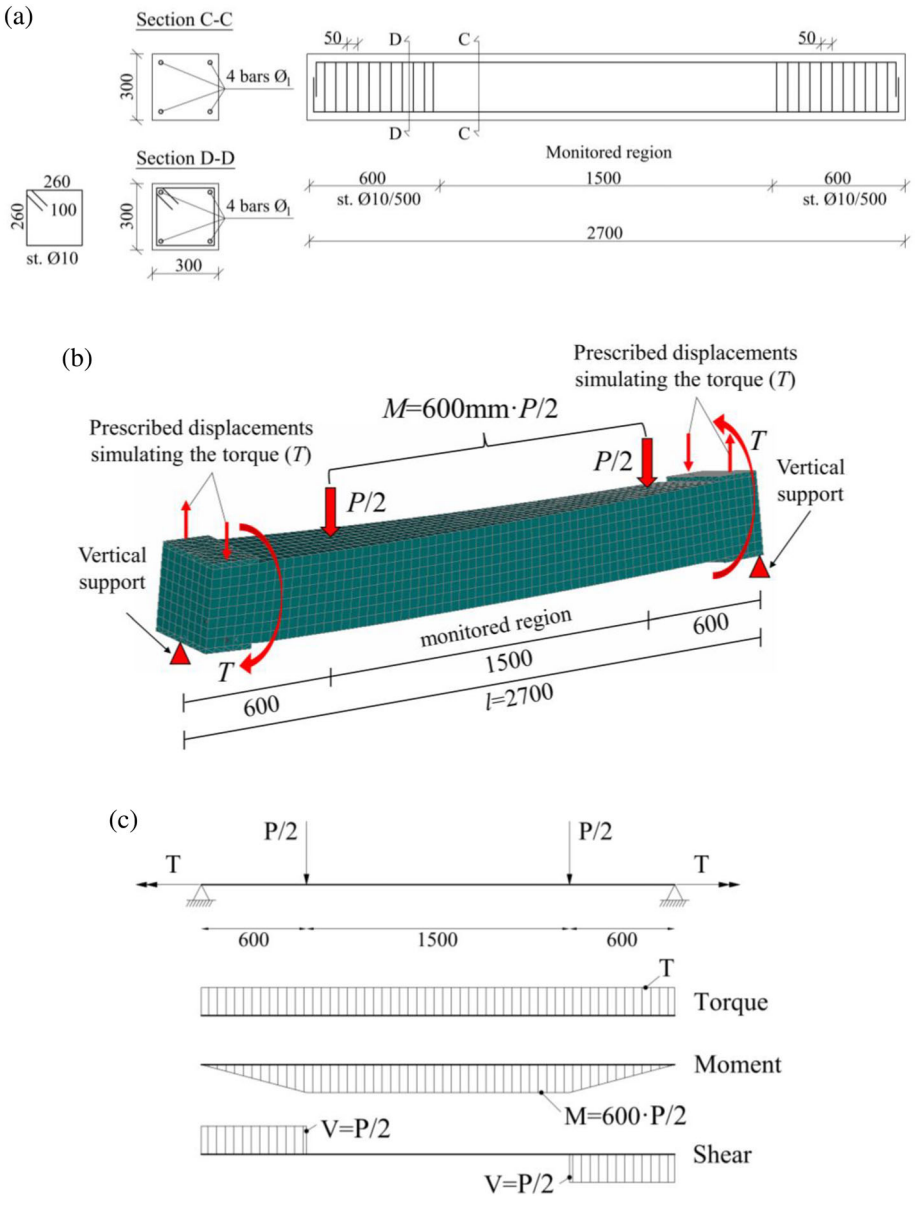

FIGURE 3 (a) Details of the pure torsion test beam; (b) typical deformed mesh of the SFRC beams without stirrups tested in the present research study; (c) simplified static scheme and internal actions considered in the numerical simulation (dimensions in mm)

hardening/softening model for concrete in compression is based on the Menétrey–William three-parameter failure surface[27] and a nonassociated flow rule of Drucker–Prager type. Strains are separated into plastic and fracturing components and a recursive iterative algorithm combines the two aforementioned models by preserving stress equivalence. The total crack width is obtained by multiplying the characteristic length with the resulting strain. The characteristic length corresponds to the crack band size as originally proposed by Bazant and Ho,[28] which is here calculated as the size of the finite element projected into the crack direction. The numerical solution was solved using the Newton–Raphson method with the tangent predictor and using the line search method. The error of residual force tolerance and the maximum number of iterations have been set equal to 0.5% and 80, respectively.

Further details on the adopted constitutive models can be found in Cervenka et al.[26] Conventional reinforcing bars (i.e., longitudinal rebars, stirrups) have been modeled by truss elements perfectly bonded to concrete. The uniaxial stress–strain law of the reinforcing steel consists of an initial linear elastic component characterized by E_s, followed by a linear strain-hardening branch with a constant slope, E_{sh} and the maximum strain $\varepsilon_{s,max}$ limiting the ductility of steel.

3.2.1 | Validation of the finite element model

To validate the model described above, the SFRC beams (refer to Table 1 for specific details of each beam) without transverse reinforcement (i.e., beam TB3 to TB10 and TB17 to TB18) tested as part of this research project and reported in a previous study[10,19] have been simulated. With regard to the concrete, the adopted material parameters used in the numerical analysis are summarized in Table 6. The mean cylindrical compressive strength (Table 2) and the tensile behavior were obtained from the characterization tests described in the accompanying paper.[19] The post-cracking uniaxial tensile stress–strain material laws related to the SFRC (i.e., FRCG25, FRCG50, FRCD25, FRCD50) forming the torsion beams have been obtained following an inverse analysis of the three-point bending tests (3PBTs) carried out according to EN 14651[24] on notched beams. The latter were modeled in ATENA using a continuum mesh consisting of the same solid elements adopted in the model of the large-scale torsion beams. Figure 4a reports the experimental nominal stress–CMOD curves together with the best-fitting curves corresponding to the uniaxial tensile stress–strain law, as shown in Figure 4b.

All materials properties can be found in Ref..[19] A strain-hardening slope (E_{sh}) of 1160 MPa and 910 MPa was implemented for the longitudinal and transversal reinforcement, respectively. To limit the tensile deformation of rebars, a maximum strain of 9.6% was used in this analysis, as obtained through material testing.

TABLE 6 Material parameters for concrete used in the finite element simulations

Parameter	Value/formulation	Unit
Initial elastic modulus	$22{,}000\cdot(f_{cm}/10)^{0.3}$[a]	MPa
Poisson's ratio	0.2	-
Tensile strength	3.5	MPa
Tensile stress–strain post-cracking law	Refer to Figure 5b	-
Characteristic size	38	mm
Compressive strain at peak	0.2	%
Uniaxial compressive strength (f_{cm})	Refer to Table 2	-
Critical compressive displacement	0.5	mm
Dilation	0	-
Tension-compression interaction	Linear[b]	-
Shear retention factor	Variable assuming 0[b]	-
Crack model	Fixed	-

[a]EN1992-1-1 Section 3.[29]
[b]Default values according Cervenka et al.[26]

Figure 5 compares the experimental torque (T)–twist (Ψ) response of the SFRC pure torsion beams with that resulting from the numerical simulations. In more detail, Figure 5a reports the response of the beams constructed with the materials FRCG25 (i.e., beams TB3 and TB4) and FRCG50 (i.e., beams TB5 and TB6), whereas Figure 5b refers to the beams constructed with concrete FRCD25 (i.e., TB7 and TB8) and FRCD50 (i.e., beams TB9, TB10, TB17, TB18).

The results shown in Figure 5 illustrate that the simulations generally provided a good estimation of the torsional behavior and response of the specimens. With regard to the capacity of the structures in resisting torsion, the simulations were capable of predicting the strength of all members within a 5%–15% tolerance.

Both the first linear branch and the torsional rigidity that characterizes the experimental response after cracking have been well captured by the numerical simulations. Despite the well-known difficulties regarding the prediction of deformations in the cracked stage of testing, the nonlinear analyses have provided reasonable estimations of the angle of twist after cracking. However, the typical horizontal plateau forming the second branch of all the actual curves was not always convincingly captured by the numerical model. Moreover, the discrepancy between the simulated and the experimental torsional rigidity after first cracking was very high for the beams

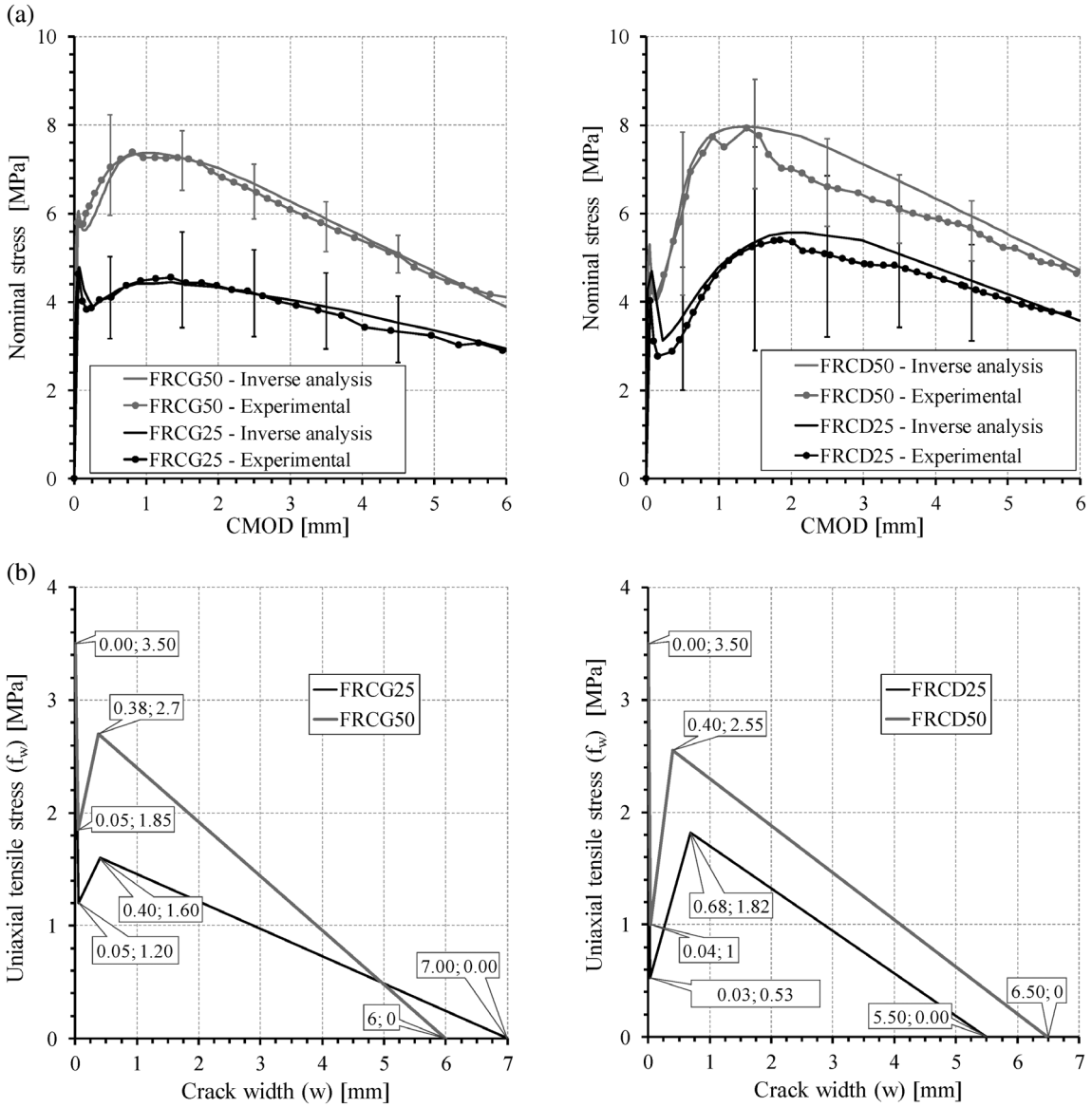

FIGURE 4 Inverse analysis of three-point bending tests (3PBTs): (a) best-fitting of the experimental nominal stress–CMOD (Crack Mouth Opening Displacement) curves and (b) corresponding uniaxial tensile stress (f_w) - crack width (w) laws of SFRC

containing longitudinal bars with a diameter ($Ø_l$) of 8 mm. These cases show that the accuracy of the model in predicting the torsional deformation of SFRC beams may be significantly reduced when considering members containing very low amounts of longitudinal reinforcement ratios and no stirrups—as previously discussed.

Aside of the considerations made above, it is worth remarking that the degree of accuracy of the numerical model is strongly related to the variability of the residual tensile strength of SFRC, which governs the torsional capacity of the beams not containing transverse reinforcement. In this regard, the scatter (i.e., a CoV varying from 10% to 40%) of the curves obtained from the 3PBTs (Figure 4a) appears consistent with the errors affecting the maximum capacities provided by the numerical torque-twist responses of the members without conventional transverse reinforcement (Figure 5).

In view of the previous considerations, the numerical model can be considered sufficiently reliable and able to provide quite accurate predictions of the torsional behavior, especially with regard to the evaluation of the torque capacity.

3.2.2 | SFRC beams under torsion and flexure: Analytical versus numerical prediction

The numerical model used in the previous section to simulate the beams subjected to pure torsion has been used here to develop a normalized interaction *T-M* domain

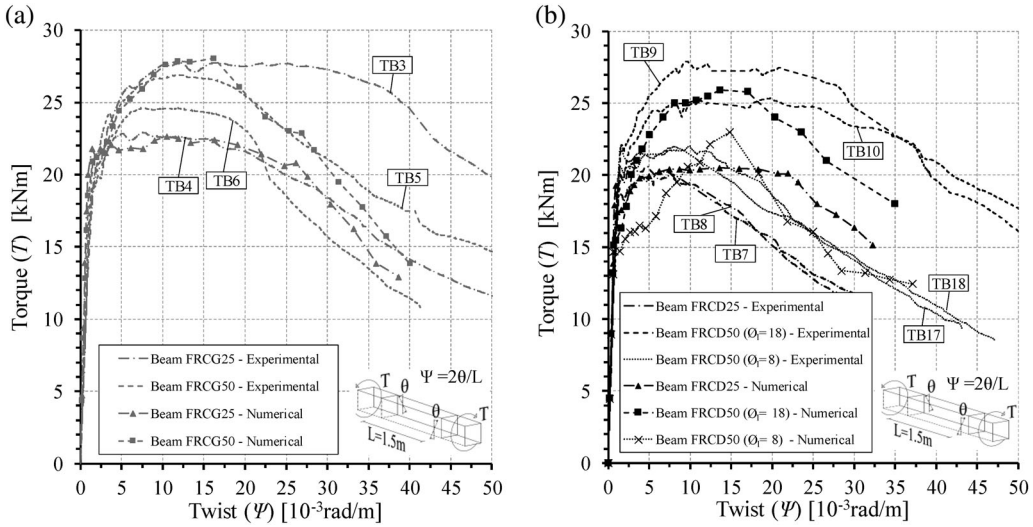

FIGURE 5 Simulation of the pure torsion beams: (a) specimens made with materials FRCG25 and FRCG50; (b) specimens made with materials FRCD25 and FRCD50

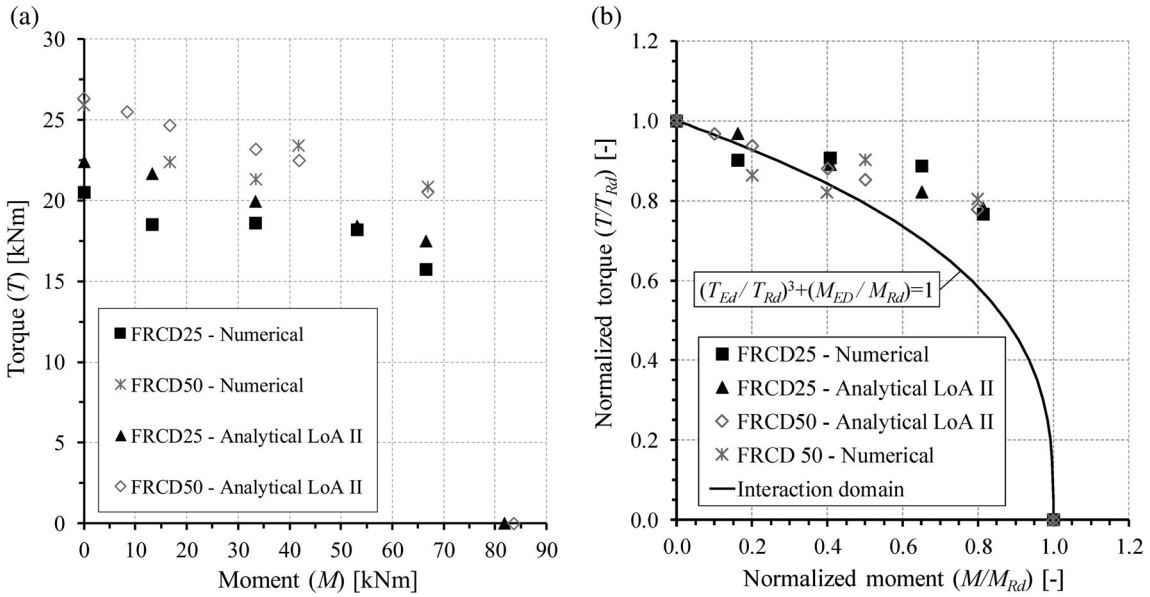

FIGURE 6 Analytical (LoA II) versus numerical analysis of beams FRCD25 and FRCD50: (a) *T*–*M* interaction curves; (b) normalized *T*–*M* curves

(Figure 6b) and to further assess the reliability of the proposed analytical model. To study the behavior of the beam under combined *T* and *M*, a bending moment was first applied to the member according to the static scheme presented in Figure 3c. Then, the torque was monotonically increased as the bending moment was kept constant. The points reported in the interaction diagram of Figure 6a correspond to the maximum torsional resistance attained by the numerical analysis. For the sake of comparison, Figure 6a also reports the interaction *T*-*M* curves developed from the analytical LoA II model presented above, for symmetrically reinforced sections. As one may note on the examination of Figure 6a, the analytical model predictions are no more than 10% greater than the corresponding numerical predictions, thus confirming its reliability even in the case of combined torsional and bending actions.

The diagram of Figure 6b reports the analytical and numerical predictions of Figure 6a in their normalized form. The latter is reasonably and conservatively fitted by the following criterion:

$$\left(\frac{T_{Ed}}{T_{Rd}}\right)^3+\left(\frac{M_{Ed}}{M_{Rd}}\right)=1, \tag{17}$$

where T_{Rd} is the ultimate pure torque (i.e., torque obtained either from the numerical simulation or through the analytical model) that may be resisted by the section (i.e., without any other applied actions), and M_{Rd} is the ultimate flexural capacity of the section, which may be determined by flexural theory. The interaction domain represented by Equation (17) is a first proposal, which needs to be further validated before being generally extended to SFRC beams different to those considered in this study. Note that the resistances predicted by the adopted interaction domain generally underestimate the numerical and analytical ones.

The safety verification of both SFRC and conventional RC structures under combined actions is not univocally addressed by structural codes, which report different interaction formulations to assess sectional resistance. Regarding SFRC structures, the lack of a significant database of experimental data for members subjected to a combination of *T-M-V* makes the calibration of an interaction domain somewhat speculative. In spite of this, it is opinion of the authors that a conservative verification of cross sections may be achieved by adopting the following formula recommended by the prEN 1992-1-1-2020[30] for RC members:

$$\sum\left(\frac{S_{Ed}}{S_{Rd}}\right)_i\le 1, \tag{18}$$

where S_{Ed}/S_{Rd} is the ratio between each individual design action (i.e., T_{Ed}, M_{Ed}, V_{Ed}) and the corresponding design resistance (i.e., T_{Rd}, M_{Rd}, V_{Rd}). It is understood that the adoption of a more refined interaction domain for SFRC members should be proposed after a thorough validation with appropriate experimental data.

4 | DESIGN EXAMPLE

A design illustration is undertaken for specimen TB11 tested in the accompanying paper.[19] The main specimen details are summarized in Tables 1 and 2 as well as in the brief description below.

The specimen is 300 mm wide by 300 mm deep and contains 50 kg/m^3 of steel fibers along with 4 × 18 mm diameter longitudinal reinforcing bars located at the corners of the cross section. The specimens also contained 6-mm-diameter stirrups spaced at 150-mm centers in the critical region. The compressive strength of the concrete is 42.6 MPa.

4.1 | Level I approximation

The LoA I solution is obtained by simplifying the three parameters θ_v, f_w, and α of Equation (16). Firstly, θ_v is taken as 43.5°, which is justified by assuming $\varepsilon_x = 0.5f_{sy}/E_s = 1.25$ mm/m. Regarding f_w, it is well known that the residual strength carried by the fibers is a function of the crack width. At the ultimate limit state, to avoid any iterations, one may adopt a constant value of $f_w = f_{Ftu} = 0.33f_{R3}$ (i.e., rigid plastic model), which is independent of the crack width. For TB11, as reported in Facconi et al,[19] $f_w = 2.21$ MPa. With respect to the term α, when stirrups are included in the section, crack widths at ultimate will be larger than the same specimen not containing the stirrups. By this, it is assumed that the influence of the aggregate interlock component to the resisting torsion is discounted. In these instances, $\alpha = 1$ is proposed.

With the simplifications made above, Equation (16) may readily be solved. The gross area of the section is $A_g = 300 \times 300 = 90{,}000$ mm^2, and the perimeter of the section is $4 \times 300 = 1200$ mm. The crushing limit of Equation (16) is therefore

$$\begin{aligned}0.25\,f_{cm}\frac{1.7\,A_g^2}{p} &= 0.25\times 42.6\times 1.7\times 90000^2/1200\\ &= 122.2\ \text{kNm}.\end{aligned} \tag{19}$$

The thickness of the equivalent hollow tube is presented in Equation (2) and is evaluated as 56.25 mm. The area of the equivalent hollow tube is therefore evaluated as $A_o = (300-56.25)(300-56.25) = 59{,}414.1$ mm^2. Noting that the top and bottom of the section is reinforced with 510 mm^2 of longitudinal reinforcing steel, Equation (16) simplifies to

$$\begin{aligned}T &= 2\times 59414.1\\ &\quad\times\min\left(\begin{array}{l}\left(\frac{28.3\times 510}{150}+1\times 56.25\times 2.21\right)\cot 43.5\\ \left(\frac{4\times 510\times 507}{1200}+1\times 56.25\times 2.21\right)\tan 43.5\end{array}\right)\\ &= 27.6\ \text{kNm}\le 122.2\ \text{kNm}.\end{aligned} \tag{20}$$

This compares well to the experimentally obtained torque of 35.63 kNm—particularly for the effort required in computation.

4.2 | Level II approximation

Alternatively, to the LoA I approach, the general (iterative) method is also provided herein using Equation (14)

TABLE 7 LoA II model iterations

Iteration	ε_x (guess) [‰]	T (guess) [kNm]	w [mm]	f_w [MPa]	θ_v [°]	f_{sl} [MPa]	f_{sv} [MPa]	v_{ci} [MPa]	T [kNm]	ε_x [‰]
1	1.71	38.4	1.042	2.23	45.3	342	510	1.18	34.0	1.51
2	1.51	34.0	0.933	2.23	44.6	303	510	1.27	35.1	1.56
3	1.56	35.1	0.960	2.23	44.8	313	510	1.24	34.8	1.55
4	1.55	34.8	0.953	2.23	44.7	310	510	1.25	34.9	1.55
5	1.55	34.9	0.955	2.23	44.7	311	510	1.25	34.9	1.55

to model the residual strength provided by the fibers. A tentative value is first required for the ultimate torque, T, and the longitudinal strain at mid-height parameter, ε_x. A suitable starting point is $T = 25$ kNm and $\varepsilon_x = 0.001$. The width of the crack is evaluated through Equation (10) and yields $w = 0.65$ mm. The principal compressive strut angle, θ_v, is determined through Equation (5) as 42.5°. The stress in the longitudinal and transverse reinforcement is evaluated through Equations (11) and (12), as 200 MPa and 510 MPa, respectively. The stress carried by the fibers, f_w, is 2.22 MPa. The shear stress accounting for aggregate interlock is determined through Equation 14 noting that the maximum aggregate particle size is 20 mm. This gives $v_{ci} = 1.59$ MPa. The resisting torque on the section is then determined through Equation (13) as 38.4 kNm. Equation (7) is used to determine ε_x and is evaluated as 0.00171. Clearly, the chosen values of T and ε_x differ from the output of the model, and so an iterative technique should be adopted until the convergence of both solutions is achieved. This process is summarized in Table 7.

After five iterations, a satisfactory convergence of ε_x and T is achieved. This compares very well to the experimentally obtained torque of 35.63 kNm. Furthermore, the mean crack width recorded in the experiment at peak torque was 1.08 mm and matches well with that (0.955 mm) produced from the analysis above.

5 | CONCLUDING REMARKS

This and the accompanying paper[19] present the results of a large-scale investigation into the behavior and design of FRC elements loaded in torsion. This article presents simplified and advanced (mechanically consistent) analytical models that are developed within three different LoAs to determine the torsion capacity of FRC beams. The LoA II analytical model is an extension of a previous model developed by the second author and is capable of predicting the torsional strength of FRC beams without stirrups. The possibility of substituting stirrups with FRC as reinforcement for torsion certainly represents an economically attractive solution for practical applications, especially in avoiding the heavy minimum torsional reinforcement generally required by structural codes.

The third LoA is based on a nonlinear FE model. The latter was used with a commercially available software for simulating the experimental results presented in the accompanying paper.[19] The third LoA and the experimental results were used as benchmark data for evaluating the approximations provided by the first two LoAs.

Based on the proposed analytical models, an interaction domain for determining the bearing capacity of a beam subjected to torsion and bending moments is proposed.

Finally, a design example provides a useful tool for better applying the proposed model.

NOTATION

a_g maximum aggregate size
A_o area enclosed by the centerline of the shear flow path
A_g gross area of beam cross section
A_s total area of the longitudinal reinforcement placed on the flexural tension side
A_{sB} total area of the longitudinal reinforcement placed at the bottom half of the beam cross section
A_{sT} total area of the longitudinal reinforcement placed at the top half of the beam cross section
A_{sl} area of each longitudinal rebar
A_{sv} area of one leg of transverse reinforcement
b total width of beam cross section
d effective depth of the beam
E_s Young's modulus of reinforcing steel
E_{sh} slope of the strain-hardening branch of the stress–strain law of reinforcing steel
f_{cm} mean cylindrical compressive strength of concrete
f_{Fts} residual tensile strength significant for serviceability conditions
f_{Ftu} residual tensile strength significant for ultimate conditions
f_R residual flexural strength obtained from bending tests on SFRC notched prisms according to EN14651:2005

$f_{sy,l}$ yield strength of longitudinal reinforcement
$f_{sy,v}$ yield strength of transverse reinforcement
f_w uniaxial tensile strength of SFRC as a function of crack width (w)
$f_{w,AS}$ uniaxial tensile strength of SFRC according to the Australian Concrete Code
$f_{w,fib}$ uniaxial tensile strength of SFRC according to *fib* Model Code 2010
h height of beam cross section
M bending moment
M_{Ed} design bending moment
M_{Rd} design resisting bending moment
N axial load normal to the member cross section
p perimeter of the beam gross section
P point load
q average shear flow
s spacing of transverse reinforcement
t_c thickness of the equivalent hollow tube section
T torque
T_{Ed} design torque
T_{exp} maximum torsional capacity resulting from experimental tests
T_{mod} resisting torque provided by the proposed analytical model
T_{Rd} design resisting torque
v_{ci} shear sliding stress acting along the crack surface
V shear force
w mean crack width
w_{SLS} crack width at Serviceability Limit State
w_u ultimate crack width
α coefficient accounting for the interaction between fibers and the aggregates in the shear transfer mechanism across cracks
$\varepsilon_{s,max}$ maximum tensile strain of reinforcing steel
ε_x total longitudinal strain at mid-depth of the member
θ_v average angle of inclination of cracks to the beam axis
ρ_s flexural reinforcement ratio
$\rho_{s,min}$ minimum flexural reinforcement ratio
$Ø_l$ diameter of longitudinal reinforcing bars
Ψ twist angle

DATA AVAILABILITY STATEMENT

The data that support the findings of this study are available from the corresponding author upon reasonable request.

ORCID

Luca Facconi https://orcid.org/0000-0003-2202-5439
Ali Amin https://orcid.org/0000-0002-9088-8634
Fausto Minelli https://orcid.org/0000-0002-4554-4285
Giovanni Plizzari https://orcid.org/0000-0003-2897-4969

REFERENCES

1. Rausch E. Design of reinforced concrete for torsion and shear (Berechnung des Eisenbetons gegen Verdhung und Abscheren). Berlin: Julius Springer-Verlag; 1929.p. 50 (in German).
2. Pfyl T. Tragverhalten von Stahlfaserbeton. PhD dissertation, IBK-report no.279. Swiss Federal Institute of technology, Switzerland. (in German); 2003.
3. Löfgren I. Fibre reinforced concrete for industrial construction – a fracture mechanics approach to material testing and structural analysis. PhD dissertation. Department of Civil and Environmental Engineering, Chalmers University of Technology, Sweden; 2005.
4. Minelli F. Plain and fiber reinforced concrete beams under shear loading: structural behavior and design aspects. PhD dissertation. Department of Civil Engineering, University of Brescia, Italy; 2005.
5. Amin A. Post cracking behaviour of steel fibre reinforced concrete: from material to structure. PhD dissertation. School of Civil and Environmental Engineering, the University of new South Wales, Australia; 2015.
6. *fib* Model Code for Concrete Structures 2010. 2013. 434.
7. AS3600, Concrete Structures. Australian Standard, Standards Association of Australia; 2018.
8. Muttoni A, Fernandez Ruiz M. Levels-of-approximation approach in codes of practice. Struct. Eng. Int. 2012;2:190–4.
9. Amin A, Bentz E. Strength of steel fiber reinforced concrete beams in pure torsion. Struct. Concr. 2018;19(3):684–94.
10. Facconi L, Minelli F, Plizzari G, Ceresa P. Experimental study on steel fiber reinforced concrete beams under pure torsion. In: Derkowski W, Gwozdziewicz P, Hojdys L, Krajewski P, Pantak M, editor. Proceedings of the fib symposium 2019 held in Krakow, Poland; Lausanne, Switzerland: International Federation for Structural Concrete (fib); 2019:1811–8.
11. Facconi L, Minelli F, Plizzari G, Ceresa P. Steel fibers for replacing minimum reinforcement in beams under torsion. Mater. Struct. 2021;54:34. https://doi.org/10.1617/s11527-021-01615-y
12. Rahal K, Collins MP. Analysis of sections subjected to combined shear and torsion – a theoretical model. ACI Struct. J. 1995;92(4):459–69.
13. Collins MP, Mitchell D. Prestressed concrete structures. Englewood Cliffs, N.J: Prentice-Hall, Inc.; 1991.p. 766.
14. Amin A, Foster S, Gilbert RI, Kaufmann W. Material characterisation of macro synthetic fibre reinforced concrete. Cem. Concr. Compos. 2017;84:124–33.
15. Minelli F, Plizzari G. Derivation of a simplified stress-crack width law for fiber reinforced concrete through a revised round panel test. Cem. Concr. Compos. 2015;58:95–104.
16. Amin A, Foster SJ, Muttoni A. Derivation of the σ-w relationship for SFRC from prism bending tests. Struct. Concr. 2015;16(1):93–105.
17. Lampert P. Ultimate strength of reinforced concrete beams in torsion and bending (Bruchwiderstand von Stahlbetonbalken unter torsion und biegung). PhD dissertation. Swiss Federal Institute of Technology, Switzerland. (in German); 1970.
18. Bentz EC, Vecchio FJ, Collins MP. Simplified modified compression field theory for calculating shear strength of reinforced concrete elements. ACI Struct. J. 2006;103(4):614–24.
19. Facconi L, Amin A, Minelli F, Plizzari G. A unified approach for determining the strength of FRC members subjected to torsion – part I: experimental investigation. *Submitted to Structural Concrete*; 2021
20. CSA. Design of concrete structures. Standard CAN/CSA A23.3–14. Mississauga, Ont: Canadian Standards Association; 2014.

21. Kaufmann W, Amin A, Beck A, Lee M. Shear stress across cracks in steel fibre reinforced concrete. Eng. Struct. 2019;186:508–24.
22. Cuenca E, Conforti A, Monfardini L, Minelli F. Shear transfer across a crack in ordinary and alkali activated concrete reinforced by different fibre types. Mater. Struct. 2020;53(2):1–15.
23. Vecchio FJ, Collins MP. The modified compression-field theory for reinforced concrete elements subjected to shear. ACI J. 1986;83(2):219–31. https://doi.org/10.14359/10416
24. EN 14651. Test method for metallic fibre concrete- measuring the flexural tensile strength (limit of proportionality [LOP], residual). Brussels, Belgium: European Committee for Standardization; 2007. p. 17.
25. Annex L. Steel Fibre Reinforced Concrete. Annex to prEN 1992-1-1 2019 D4 - CEN TC 250/SC2/WG1/TG2
26. Cervenka V, Jendele L, Cervenka J. ATENA program documentation—part 1: theory. Prague: Cervenka Consulting; 2007.
27. Menetrey P, Willam KJ. Triaxial failure criterion for concrete and its generalization. ACI Struct. J. 1995;92(3):311–8.
28. Bazant ZP, Oh BH. Crack band theory for fracture of concrete, materials and structures. RILEM. 1983;16:155–77.
29. EN 1992-1-1 Eurocode 2: Design Of Concrete Structures - Part 1–1: General Rules and Rules For Buildings. E. for standardization. Brussels, EN, CEN; 2005, EC2.
30. prEN 1992-1-1 (2020). Eurocode 2: Design of concrete structures – Part 1–1: General rules – Rules for buildings, bridges and civil engineering structures

AUTHOR BIOGRAPHIES

Luca Facconi, PhD, Assistant Professor, Department of Civil, Environmental, Architectural Engineering and Mathematics (DICATAM), University of Brescia, Italy.

Ali Amin, Senior Lecturer, School of Civil Engineering, The University of Sydney, Australia.

Fausto Minelli, PhD, Associate Professor, Department of Civil, Environmental, Architectural Engineering and Mathematics (DICATAM), University of Brescia, Italy.

Giovanni Plizzari, Professor, Department of Civil, Environmental, Architectural Engineering and Mathematics (DICATAM), University of Brescia, Italy.

How to cite this article: Facconi L, Amin A, Minelli F, Plizzari G. A unified approach for determining the strength of FRC beams subjected to torsion–Part II: Analytical modeling. Structural Concrete. 2021;1–18. https://doi.org/10.1002/suco.202100162